Journal of Power Sources 195 (2010) 6977–6981

Contents lists available at ScienceDirect

Journal of Power Sources

journal homepage: www.elsevier.com/locate/jpowsour

Short Communication

Capacitance decay of nanoporous nickel hydroxide

Guangxia Hu [a], Chunxiang Li [b], Hao Gong [a,*]

[a] Department of Materials Science & Engineering, National University of Singapore, 10 Kent Ridge Crescent, Singapore 119260, Singapore
[b] Advanced Materials Technology Centre, Singapore Polytechnic, 500 Dover Road, Singapore 139651, Singapore

ARTICLE INFO

Article history:
Received 17 February 2010
Received in revised form 16 March 2010
Accepted 22 March 2010
Available online 3 April 2010

Keywords:
Nanoporous nickel hydroxide
Capacitance decay
High current density
Supercapacitor
Phase change

ABSTRACT

Nanoporous nickel hydroxide $Ni(OH)_2$ coated on nickel foam by using a chemical bath deposition method shows a high specific capacitance of 2200 F g^{-1} at a discharging current density of 1 A g^{-1}. After 500 charge–discharge cycles, the specific capacitance is stabilized at 1470 F g^{-1}, and there is only a 5% fall in specific capacitance during the following 1500 cycles. The relationship between the capacitance decay and changes in the microstructure and morphology of nanoporous $Ni(OH)_2$ is investigated. The results show that phase transformation and the growth of particle/crystal size, rather than the formerly proposed flaking off of $Ni(OH)_2$, are the major factors contributing to the capacitance decay.

1. Introduction

Nickel hydroxide ($Ni(OH)_2$) has been used for many decades as an active material for the positive electrode of batteries. These nickel-based batteries can perform well at relatively low discharge rates (0.1–1 C). At very high discharge rates (>10 C), however, only a few percent of the storage capacity can be used [1]. At high discharge rates/current densities, the best energy-storage device is the supercapacitor. Well-developed carbon-based supercapacitors (electric double-layer capacitors) have very high discharge current densities, but they suffer from a low energy density or a low specific capacitance of about 200 F g^{-1} [2].

In recent years, nanosized $Ni(OH)_2$, which can function well at high discharge current densities, has been identified as a very promising material for supercapacitors [3–10]. Two types of energy-storage mechanism play a role in a supercapacitor, namely, non-faradic charging as in electric double-layer capacitors and Faradaic charging similar to the processes in batteries. Studies [11,12] show that high current density discharge performance is improved greatly by using nanostructured $Ni(OH)_2$ because of the high specific surface area, fast redox reaction and shortened diffusion path in the solid phase. Cheng et al. [8] reported a specific capacitance of ~696 F g^{-1} for sol–gel-derived $Ni(OH)_2$ xerogels, i.e., a performance that is significantly higher than that of well-developed carbon-based materials. Yuan et al. [13] reported a specific capacitance of ~710 F g^{-1} for spherical superstructured $Ni(OH)_2$. Lang et al. [5] and Yang et al. [14] further reported a higher specific capacitance (>2000 F g^{-1}) for loosely packed, nanoflake $Ni(OH)_2$ structures. Although a high specific capacitance is achieved, nanostructured $Ni(OH)_2$ suffers from significant capacitance decay during charge–discharge cycles and thereby prevents it from industry applications such as electrical vehicles and hybrid electrical vehicles. Some researchers propose that the capacitance decay may be due to the flaking off of $Ni(OH)_2$ [14]. There is no strong evidence to support this view, however, and no other possible reasons have been advanced, according to the best of our knowledge. A systematic investigation is needed to alleviate the ambiguities for a better understanding of this important phenomenon and thus pave the way to industrial applications of high capacitance $Ni(OH)_2$ supercapacitors.

In this work, a $Ni(OH)_2$ film with interconnected nanoflakes is deposited directly on a nickel foam substrate, and a high specific capacitance of up to 2200 F g^{-1} is achieved. The decay in capacitance during charge–discharge cycles is studied systematically by means of multi-characterization techniques including XRD, SEM, TEM, and electrochemical methods. Capacitance decay behaviour under different current regimes is also examined.

2. Experimental details

The solution for chemical bath deposition (CBD) was prepared by mixing 40 mL of 1 M nickel sulfate, 30 mL of 0.25 M potassium persulfate, 10 mL of aqueous ammonia (22–24% NH_3), and 20 mL of deionized water in a 250 mL Pyrex beaker at room temperature. The Ni foam substrate was chemically cleaned with acetone, methanol,

* Corresponding author. Tel.: +65 65164632; fax: +65 68742081.
E-mail address: msegongh@nus.edu.sg (H. Gong).

0378-7753/$ – see front matter © 2010 Published by Elsevier B.V.
doi:10.1016/j.jpowsour.2010.03.093

and deionized water. Clean substrates were dried in flowing nitrogen. Cyclic voltammetry (CV) and charge–discharge measurements were carried out in a three-compartment system containing a 1 M KOH electrolyte solution, a saturated calomel electrode (SCE) as the reference electrode, and a Pt foil counter-electrode. The weight of the electrode was measured with a Mettler Toledo X205DU Microbalance (sensitivity: 0.01 mg; repeatability: 0.015 mg). Before each weighing, the samples were washed in deionized water and then dried at 60 °C for 2 h. The CV measurements of the $Ni(OH)_2$–Ni foam electrode were performed using a Solartron 1267 potentiostat coupled with Corrware (Scribner Associates) at a scanning rate of 1 mV s^{-1} between 0 and 0.55 V vs. SCE was at room temperature (25 °C). X-ray diffraction (XRD) spectra were obtained with a BRUKER AXS instrument (model D8 ADVANCE, $\lambda_{Cu,K\alpha}$ = 0.154060 nm). The morphology of the electrodes was analyzed by means of scanning electron microscopy (SEM, FE-XL 30). Transmission electron microscopy (TEM, JEOL2000FX) was employed to investigate the microstructure of the $Ni(OH)_2$.

3. Results and discussion

The XRD pattern of the $Ni(OH)_2$ powder prepared by CBD is presented in Fig. 1a. Three peaks belonging to α-$Ni(OH)_2$ (JCPDF #22-0444) (0 0 1) (2θ = 11.634°), (0 0 2) (2θ = 23.771°) and (1 1 0) (2θ = 33.666°) are observed. A TEM image of the $Ni(OH)_2$ sample is given in Fig. 1b and reveals slices of α-$Ni(OH)_2$ with dimensions of ~50–200 nm. The inset of Fig. 1b is a selected area of the electron

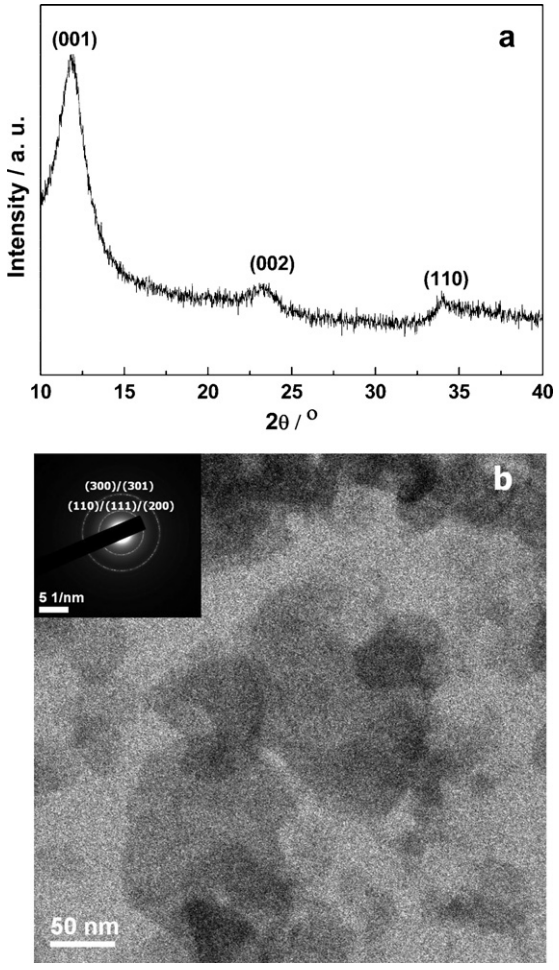

Fig. 1. (a) XRD spectrum of $Ni(OH)_2$ powder and (b) TEM image of $Ni(OH)_2$ sample; inset is selected area electron diffraction (SAED) pattern of $Ni(OH)_2$ from electrode.

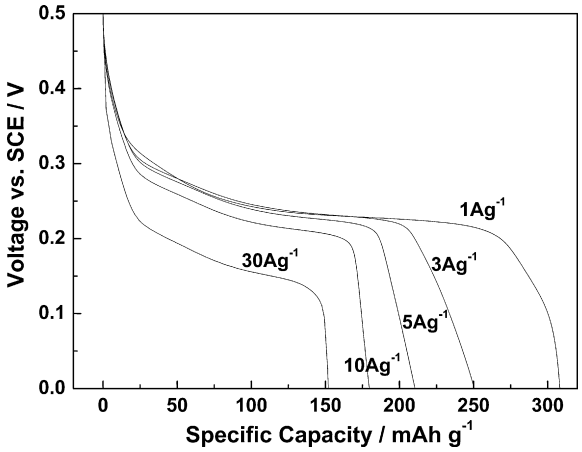

Fig. 2. Discharge behaviour of $Ni(OH)_2$–Ni foam electrode measured (charging at 3 A g^{-1} to 0.5 V vs. SCE) in potential range from 0.5 to 0 V vs. SCE at current density of 1, 3, 5, 10 and 30 A g^{-1} in 1 M KOH solution.

diffraction (SAED) pattern of a typical slice (with the incident electron beam perpendicular to the slice). The pattern reveals that the sample is α-$Ni(OH)_2$, in agreement with XRD analysis. The rings in the SAED pattern can be indexed as α-$Ni(OH)_2$ (1 1 0)/(1 1 1)/(2 0 0) and (3 0 0)/(3 0 1) planes. It is interesting to find that there are no (0 0 1) and (0 0 2) rings in the SAED pattern, suggesting that the slice plane is (0 0 1). The formation of (0 0 1) slices is probably due to the low surface formation energy of the (0 0 1) surface of α-$Ni(OH)_2$.

A constant-current discharge experiment was conducted to obtain the specific capacitance of $Ni(OH)_2$. The electrodes were charged to 0.5 V at a constant current density of 3 A g^{-1} before discharging. The discharge behavior, is shown in Fig. 2, i.e., the potential vs. specific capacity of the $Ni(OH)_2$ measured at discharging current densities of 1, 3, 5, 10 and 30 A g^{-1} in 1 M KOH. The corresponding specific capacitance of the sample is calculated from

$$C = \frac{I \cdot \Delta t}{m \cdot \Delta V}, \quad (1)$$

where I is the discharging current; Δt is the total discharging time; m is the mass; ΔV is the total potential drop; C is the specific capacitance. The as-deposited $Ni(OH)_2$–Ni foam electrode (0.5 cm × 0.5 cm) contains 0.48 mg $Ni(OH)_2$. The specific capacitance values are calculated to be 2222, 1804, 1516, 1299 and 1103 F g^{-1}, which correspond to the discharge current densities of 1, 3, 5, 10 and 30 A g^{-1}, respectively. The high specific capacitance achieved suggests that nanoporous $Ni(OH)_2$ in the electrode is electrochemically accessible and contributes to the capacitance [15]. The decrease in capacitance with increase in discharge current suggests an increasing involvement of polarization, a phenomenon that results in a low utilization of the active materials at higher charge/discharge currents [16], in agreement with other studies [5,17].

Since a long cycle-life is critical to supercapacitor applications, a cycle test was carried out to examine the service life of the electrode. The $Ni(OH)_2$–Ni foam electrode was charged and discharged at a current density of 3 A g^{-1} in the 0–0.50 V range vs. SCE up to 2000 cycles. The specific capacitance at the beginning and after each 500 cycles at 3 A g^{-1} is given in Fig. 3; the capacitance was measured at discharge current densities of 1, 3, 5, 10 and 30 A g^{-1} (charge to 0.5 V at 3 A g^{-1}, for all cases). Decay of capacitance with performing cycles is clearly seen in Fig. 3. After 500 charging–discharging cycles at 3 A g^{-1}, the specific capacitances dropped to 1502, 1435, 1301, 1173 and 1050 F g^{-1}, measured at discharging current densities of 1, 3, 5, 10 and 30 A g^{-1}, respectively. After 2000 cycles, the specific capacitances became 1387, 1295, 1169, 991 and 725 F g^{-1}, at 1, 3, 5,

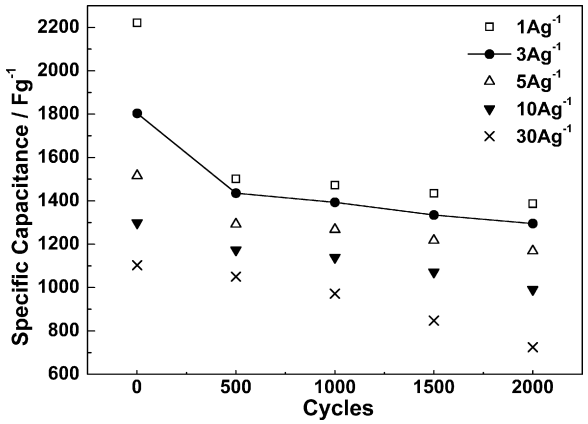

Fig. 3. Relationship between capacitance retention and cycle number of $Ni(OH)_2$–Ni foam electrode at different specific discharge currents.

Table 1
Relative capacitance decay after 500 cycles (range I: 1–500 cycles) and 2000 cycles (range II: 500–2000 cycles), measured with different discharging current densities.

Discharging current density ($A\,g^{-1}$)	Relative capacitance drop (%)	
	After 500 cycles	After 2000 cycles
1	32.4	7.7
3	20.5	9.8
5	14.2	10.1
10	9.7	15.5
30	4.8	31.0

10 and 30 $A\,g^{-1}$, respectively. Since the flaking off of $Ni(OH)_2$ from electrode has been considered to be the major cause of the fall in capacitance [13], the weight measurement was carried out before and after 2000 cycles. The electrode weight before cycling and after 2000 cycles showed no detectable loss using a balance with 0.01 mg sensitivity, suggesting that weight loss is not the major determinant of capacitance decay. Therefore, the significant capacitance decay during cycling should be attributed to other factors. The following will focus mainly on understanding the factors that contribute to capacitance decay.

A careful inspection of Fig. 3 reveals that the capacitance decay behaviour can be divided into two ranges, namely, 1–500 cycles (range I) and 500–2000 cycles (range II), because the gradients of the lines joining the data are different in these two ranges. Table 1 lists the relative fall in specific capacitance for the two ranges of cycles at different discharging current densities. For range I, the relative capacitance drop becomes less with increase in discharge current density, e.g., a 32.4% capacitance drop occurs at a discharge current density of 1 $A\,g^{-1}$, but there is only a 4.8% drop at 30 $A\,g^{-1}$ after 500 cycles. It is well accepted that both the surface and bulk redox activities play major roles at a low discharge current density, but the surface activity becomes dominant at a high discharge current density. The observation of a 32.4% capacitance decay at 1 $A\,g^{-1}$ and only a 4.8% capacitance decay at 30 $A\,g^{-1}$ may indicate that a change in the $Ni(OH)_2$ material, rather than a decrease in surface area, is mainly responsible for the capacitance decay phenomenon after 500 cycles in range I. For range II, the relative capacitance drop increases with the discharge current density, i.e., totally different from the trend in range I. The capacitance falls 7.7% at a

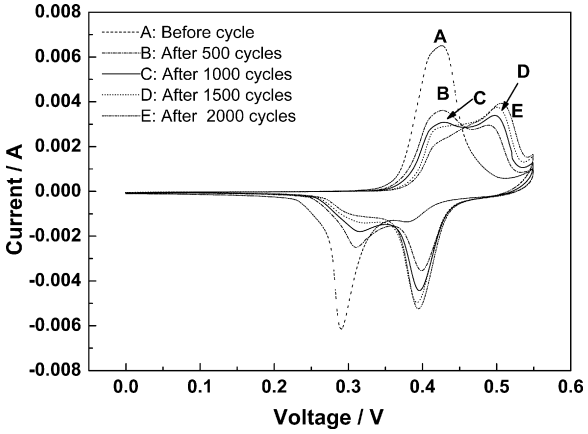

Fig. 4. Cyclic voltammetry curves at 1 mV s^{-1} within a potential window of 0–0.55 V vs. SCE in 1 M KOH. A, before cycles; B, after 500 cycles; C, after 1000 cycles; D, after 1500 cycles; E, after 2000 cycles.

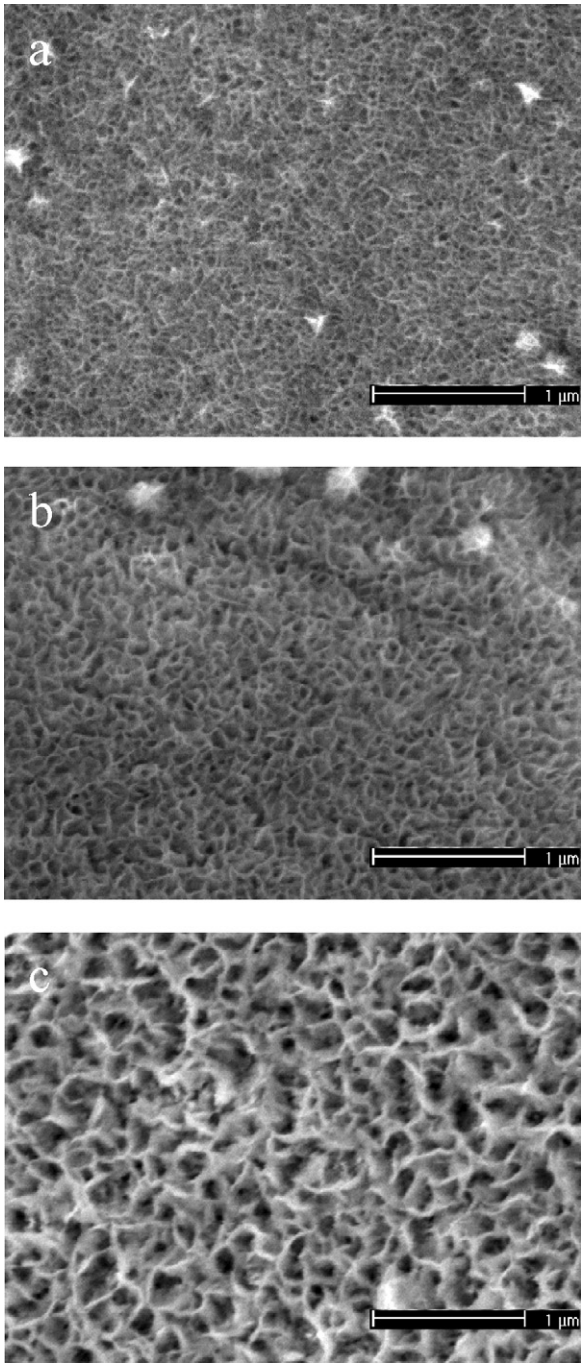

Fig. 5. SEM images (20,000×) of Ni(OH)–Ni foam electrode: (a) as-deposited; (b) after 500 cycles; (c) after 2000 cycles.

discharge current density of $1\,A\,g^{-1}$, but 31.0% at $30\,A\,g^{-1}$. Such a phenomenon may suggest that a significant decrease in surface area, rather than a change in material, is dominant in range II of 500–2000 cycles.

To investigate the change in material property, cyclic voltammetry experiments were performed. The CV curves of a $Ni(OH)_2$–Ni foam electrode at different cycles at a scan rate of $1\,mV\,s^{-1}$ in 1 M KOH are given in Fig. 4. In the first CV scan (Fig. 4, curve A), an oxidation current peak is found at ~420 mV, and two partly overlapping reduction current peaks at 290 and 378 mV. Such peaks are related to Faradaic reactions of $Ni(OH)_2$ described by the following well-accepted reaction [18].

$$Ni(OH)_2 + OH^- \leftrightarrow NiOOH + H_2O + e^- \quad (2)$$

Based on a Bode diagram [19] and the as-deposited α-$Ni(OH)_2$ film, the anodic peak at 420 mV is attributed to a transformation of α-$Ni(OH)_2$ to γ-NiOOH. The cathodic peak at 378 mV is attributed to a phase change from γ-NiOOH to β-$Ni(OH)_2$ [20]. The cathodic peak at 290 mV is due to a reverse process where γ-NiOOH and β-$Ni(OH)_2$ revert back to α-$Ni(OH)_2$. Curve B in Fig. 4, for the sample cycled 500 times, presents distinctly different features from curve A, namely, an additional anodic peak at 500 mV and an additional cathodic peak at 397 mV. The presence of additional peaks indicates the formation of a new phase during the charge–discharge process. It is further noticed in Fig. 4 that the change in the features of the CV curves becomes much less significant after the first 500 cycles, suggesting that the change in $Ni(OH)_2$ material occurs mainly during these cycles. Subsequently, the intensities of the additional peaks at 500 and 397 mV still increase slightly with cycling and are accompanied by a decrease in the intensity of the anodic peak at 420 mV and of the cathodic peak at 290 mV (curves C, D, and E). The small change in the intensity of these peaks may indicate a continuous minor conversion of α-$Ni(OH)_2$ and γ-NiOOH phases into new phases. It is known that the anodic peak of β-$Ni(OH)_2$ has a higher potential with respect to that of α-$Ni(OH)_2$ in the anodic direction [21]. It is possible that the appearance of the new peaks indicates the formation of β-$Ni(OH)_2$. To verify the change in the sample and the formation of new phases, SEM and TEM analyses were performed.

The surface morphologies of $Ni(OH)_2$–Ni foam electrodes before and after 500 and 2000 cycles are shown in Fig. 5. The surface of the as-deposited electrode is highly porous and composed of small interconnected nanoflakes. Changes in the morphology of the cycled $Ni(OH)_2$ film can be observed Increases in flake size, flake thickness and pore size become more and more obvious, especially after the samples have been cycled for 500–2000 times (see Fig. 5). These morphology changes indicate that a mass transfer and

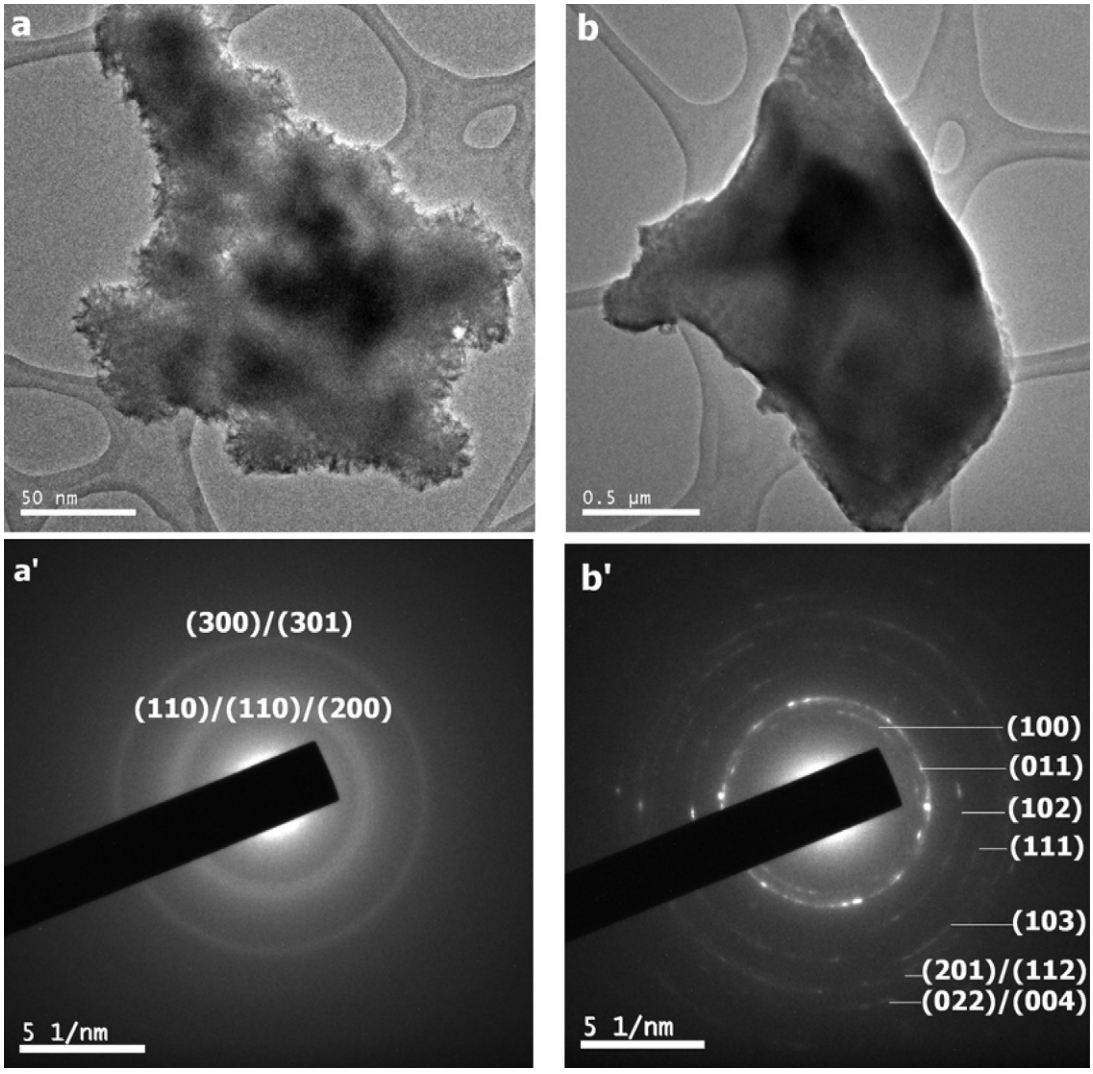

Fig. 6. TEM images of $Ni(OH)_2$ film after cycling 2000 times: (a) TEM image and (a′) SAED and (a″) HRTEM image of one flake; (b) TEM image, and (b′) SAED.

a recrystallization process occur during the cycling process and lead to particle growth in the nanoporous $Ni(OH)_2$ film. The increase in particle size leads to decrease in surface area.

The change in film microstructure during cycling was investigated by means of TEM. Fig. 6 shows TEM and SAED results for two typical types of flake identified in the as-deposited and 2000 cycled $Ni(OH)_2$ samples. The flake size shown by TEM (Fig. 6b) is ~10 times larger than that for SAED (Fig. 6a). The flake size in Fig. 6a is similar to that of α-$Ni(OH)_2$ flakes in Fig. 1. The larger flake size in Fig. 6b is similar to those appearing in Fig. 5c. Analysis of the SEM images in Fig. 5 shows that the flakes not only become larger but also thicker. The TEM images in Fig. 6b also demonstrate that the flakes are much thicker than the flakes in Fig. 6a. The SAED patterns taken form these two flakes (Fig. 6a′ and b′), reveal the phases of the materials. The rings in the SAED pattern in (a′) can be indexed as the (1 1 0)/(1 1 1)/(2 0 0) and (3 0 0)/(3 0 1) planes of α-$Ni(OH)_2$. This confirms the XRD results that such a type of flake has the same structure as that of the as-deposited α-$Ni(OH)_2$. The rings in the SAED pattern in Fig. 6b′ can be indexed as the (1 0 0), (0 1 1), (1 0 2), (1 1 1), (1 0 3), (2 0 1)/(1 1 2) and (0 2 2)/(0 0 4) planes of β-$Ni(OH)_2$, in agreement with the JCPDF #73-1520.

Since α-$Ni(OH)_2$ is known to be unstable in the presence of water and alkali, in which it transforms to β-$Ni(OH)_2$ [22], it is necessary to determine whether the transformation from α-$Ni(OH)_2$ to β-$Ni(OH)_2$ is due to the reaction of KOH with α-$Ni(OH)_2$. The as-deposited α-$Ni(OH)_2$ sample was dipped in 1 M KOH for 6 days. No phase change was detected, suggesting that the transformation cannot be due to the reaction of α-$Ni(OH)_2$ with KOH. Then the phase change from α-$Ni(OH)_2$ to β-$Ni(OH)_2$ should occur during the charge–discharge process.

It has been reported [23,24] that the transformation from α-$Ni(OH)_2$/γ-NiOOH redox couple to β-$Ni(OH)_2$/β-NiOOH redox couple [23,24] can lead to a capacitance decay because the oxidation state of nickel in β-NiOOH is lower than that of γ-NiOOH (β-NiOOH ~3; γ-NiOOH ~3.5). Therefore, the anodic peak at 500 mV and the cathodic peak at 397 mV shown in Fig. 4 could be attributed to the β-$Ni(OH)_2$/β-NiOOH redox couple. This is consistent with the different redox potentials of α-$Ni(OH)_2$/α-NiOOH and β-$Ni(OH)_2$/β-NiOOH [25], because β-$Ni(OH)_2$ is converted to β-NiOOH at a higher potential than α-$Ni(OH)_2$ to γ-NiOOH [21].

The above results and discussion reveal that the nanoporous $Ni(OH)_2$ film undergoes a phase change from α-$Ni(OH)_2$ to β-$Ni(OH)_2$ as well as a growth of particle and crystal size. These changes are responsible for the capacitance decay during the charge–discharge process. Analysis of capacitance change, CV behaviour, morphology and microstructure of the samples suggests that there is a competition between the phase change and the growth of particle and crystal size in the capacitance decay mechanism. Although the phase change from α-$Ni(OH)_2$ to β-$Ni(OH)_2$ reduces the capacitance of $Ni(OH)_2$, it can improve the utilization of the active materials at high polarization states by increasing the reduction potential. The growth of particle and crystal size enhances the polarization of electrode because the resistance can be increased due to the surface area decrease of $Ni(OH)_2$. The colour of the cycled $Ni(OH)_2$–Ni foam electrode becomes darker after certain number of cycles (~500). It is known that the coloured state of $Ni(OH)_2$ is associated with the existence of β-NiOOH or γ-NiOOH in film [26,27]. As indicated by Eq. (2), NiOOH will be consumed after an ideal discharging process. The darker colour after discharge indicates, however, that NiOOH is still present in the electrode due to incomplete film reduction. Therefore, incomplete film reduction can also contribute to the decay in capacitance.

4. Conclusions

A $Ni(OH)_2$–Ni foam electrode has been fabricated by using a CBD method to deposit a nanoporous $Ni(OH)_2$ layer on a Ni foam substrate. A high specific capacitance of 2222, 1804, 1516, 1299 and 1103 $F g^{-1}$ is obtained at a current density of 1, 3, 5, 10 and 30 $A g^{-1}$, respectively. After 2000 cycles, the specific capacitance is 1387, 1295, 1169, 991 and 725 $F g^{-1}$ at a current density of 1, 3, 5, 10 and 30 $A g^{-1}$, respectively. A phase transformation and the growth of particle and crystal size are identified after cycling. The results reveal that the phase transformation is the major contributor to the capacitance decay at relatively low discharge current densities, whereas the growth of particle and crystal size is the major contributor to the capacitance decay at higher discharge current densities. These findings contradict proposals in the literature that flaking off of $Ni(OH)_2$ is responsible for capacitance decay. At the same time, the existence of incomplete film reduction can also contribute to capacitance decay.

Acknowledgements

The authors are grateful to the Agency of Science, Technology and Research (A*STAR), Singapore, and the National University of Singapore (NUS) for financial support (grant R-284-000-067-592).

References

[1] A. Green, S.C. Jehoulet, The Battcon 2002 Proceedings Battcon 2002 Conference, Ft. Lauderdale, FL.
[2] L.L. Zhang, X.S. Zhao, Chem. Soc. Rev. 38 (2009) 2520.
[3] M. Jayalakshmi, K. Balasubramanian, Int. J. Electrochem. Sci. 3 (2008) 1196.
[4] J. Lang, L. Kong, W. Wu, Y. Luo, L. Kang, Chem. Commun. 35 (2008) 4213.
[5] J. Lang, L. Kong, W. Wu, M. Liu, Y. Luo, L. Kang, J. Solid State Electrochem. 13 (2009) 333.
[6] F. Ferreira, M.H. Tabaanics, M.C.A. Fantini, I.C. Faria, A. Gorenstein, Solid State Ionics 86–88 (1996) 971.
[7] M. Wu, Y. Huang, C. Yang, J. Electrochem. Soc. 15 (2008) A798.
[8] J. Cheng, G. Cao, Y. Yang, J. Power Sources 47 (2006) 89.
[9] U.M. Patil, R.R. Salunkhe, K.V. Gurav, C.D. Lokhande, Appl. Surf. Sci. 255 (2008) 2603.
[10] U.M. Patil, K.V. Gurava, V.J. Fulari, C.D. Lokhandea, Oh Shim Joo, J. Power Sources 188 (2009) 338.
[11] X. He, W. Pu, H. Cheng, C. Jiang, C. Wan, Energy Convers. Manage. 47 (2006) 1879.
[12] X. Liu, L. Yu, J. Power Sources 128 (2004) 32.
[13] C. Yuan, X. Zhang, L. Su, B. Gao, L. Shen, J. Mater. Chem. 19 (2009) 5772.
[14] G. Yang, C. Xu, H. Li, Chem. Commun. 48 (2008) 6537.
[15] B.E. Conway, Electrochemical Supercapacitors: Scientific Fundamentals & Technological Applications, Plenum Press, New York, 1999.
[16] C. Yuan, B. Gao, X. Zhang, J. Power Sources 173 (2007) 606.
[17] R. Kötz, M. Carlen, Electrochim. Acta 45 (2000) 2483.
[18] L. Cao, L.B. Kong, Y.Y. Liang, H.L. Li, Chem. Commun. 14 (2004) 1646.
[19] H. Bode, K. Dehmelt, J. Witte, Electrochim. Acta 11 (1966) 1079.
[20] N. Sac-Epée, M.R. Palacin, A. Delahaye-Vidal, Y. Chabre, J. Tarascon, J. Electrochem. Soc. 145 (1998) 1434.
[21] Q. Yi, J. Zhang, W. Huang, X. Liu, Catal. Commun. 8 (2007) 1017.
[22] D. Singh, J. Electrochem. Soc. 145 (1998).
[23] R.S. Jayashree, P.V. Kamath, J. Appl. Electrochem. 31 (2001) 1315.
[24] P.V. Kamath, M. Dixit, L. Indira, A.K. Shukla, V.G. Kumar, N. Munichanduaiah, J. Electrochem. Soc. 141 (1994) 2956.
[25] B. Liu, Y. Zhang, H. Yuan, H. Yang, E. Yang, J. Hydrogen Energy 25 (2000) 333.
[26] Y.L. Lo, B.J. Hwang, Langmuir 14 (1998) 944.
[27] M.A. Vidales-Hurtado, A. Mendoza-Galván, Solid State Ionics 179 (2009) 2065.